Smart Structures and Systems, *Vol. 30, No. 2 (2022) 183-193*
https://doi.org/10.12989/sss.2022.30.2.183

Thermomechanical and electrical resistance characteristics of superfine NiTi shape memory alloy wires

Hui Qian [1a], Boheng Yang[*1], Yonglin Ren [1] and Rende Wang [2]

[1] *School of Civil Engineering, Zhengzhou University,100 Science Avenue, Zhengzhou City, the People's Republic of China*
[2] *Henan Haoze Electronics Co., Ltd., 7 Mengzhou Hi-tech Pioneer Park, Jiaozuo City, the People's Republic of China*

(*Received July 29, 2021, Revised April 26, 2022, Accepted May 21, 2022*)

Abstract. Structural health monitoring and structural vibration control are multidisciplinary and frontier research directions of civil engineering. As intelligent materials that integrate sensing and actuation capabilities, shape memory alloys (SMAs) exhibit multiple excellent characteristics, such as shape memory effect, superelasticity, corrosion resistance, fatigue resistance, and high energy density. Moreover, SMAs possess excellent resistance sensing properties and large deformation ability. Superfine NiTi SMA wires have potential applications in structural health monitoring and micro-drive system. In this study, the mechanical properties and electrical resistance sensing characteristics of superfine NiTi SMA wires were experimentally investigated. The mechanical parameters such as residual strain, hysteretic energy, secant stiffness, and equivalent damping ratio were analyzed at different training strain amplitudes and numbers of loading–unloading cycles. The results demonstrate that the detwinning process shortened with increasing training amplitude, while austenitic mechanical properties were not affected. In addition, superfine SMA wires showed good strain–resistance linear correlation, and the loading rate had little effect on their mechanical properties and electrical resistance sensing characteristics. This study aims to provide an experimental basis for the application of superfine SMA wires in engineering.

Keywords: ER sensing; mechanical properties; shape memory effect; superelasticity; superfine SMA wire

1. Introduction

Shape memory alloys (SMAs) are crucial intelligent materials with both sensing and actuation functions. They exhibit a unique shape memory effect (SME) and superelasticity (SE) because of the phase transformation between austenite and martensite. Owing to their good mechanical properties, corrosion resistance, biocompatibility, high damping, and resistance sensing properties, SMAs have been used in many fields, such as aerospace, mechanical electronics, biomedical, and civil engineering (Janke *et al*. 2005, Song *et al*. 2006, Lester *et al*. 2015, Zadafiya *et al*. 2021).

SMAs are widely used in actuators (Dhanalakshmi *et al*. 2011, Lee *et al*. 2018, 2020, Shi *et al*. 2014) and sensors (Nahm *et al*. 2005, Song *et al*. 2007, Cui *et al*. 2010, Nakshatharan and Dhanalakshmi 2014) because of their excellent reset ability and resistive sensing characteristics. However, SME is related to the elemental composition, stress, and ambient temperature of the material, and its mechanical behaviors are relatively complex. Martensitic SMAs exhibit high energy dissipation capability, while austenitic SMA shows excellent self-centering capabilities but lesser energy dissipation. Moreover, both types guarantee a very high fatigue resistance to large strain cycles, together with a stable and repeatable cyclic behavior.

Considerable research efforts have been devoted to investigating the mechanical properties of SMA under different conditions. Churchill *et al*. (2010) conducted a series of experiments on shape memory wires to demonstrate the sensitivities of the superelastic response to the typical ambient media (water vs. air) and loading rate, which show how latent heat interactions between the SMA and its surroundings lead to loading-rate effects and complex phase front kinetics. Dolce and Cardone (2001a, b) investigated the mechanical behaviors of several specimens of NiTi SMA through experimental test programs, and they described and analyzed the results of the tests in terms of mainly four fundamental mechanical quantities: secant stiffness, energy loss, residual strain, and equivalent damping. The experimental results show that SMA bars and wires have great potential for use in seismic devices owing to their considerable energy dissipation capacity and outstanding fatigue resistance. Desroches *et al*. (2004) compared and analyzed the mechanical properties of SMA wires and bars under the circulating condition, where both SMA wires and bars showed excellent SE. Suhail *et al*. (2021) have analyzed and compared the thermomechanical behavior of NiTi-based SMAs at constant stress but variable temperature loading. The results showed that a large forward transformation strain at a constant stress of 600 MPa, in the range of 5–11%, is produced when the temperature is lowered to or below room temperature. Casciati and Marzi (2010) investigated the creep

*Corresponding author, MA. SC. Student,
E-mail: 22b333004@stu.hit.edu.cn
[a] Professor, E-mail: qianhui@zzu.edu.cn

ISSN: 1738-1584 (Print), 1738-1991 (Online)

phenomenon of two different alloys, a classical NiTi alloy and a Cu-based alloy, and experimentally measured the fatigue characteristics of the Cu-based alloy. DesRoches *et al*. (2004) tested SMA wires and bars to evaluate the effect of bar size and loading history on the strength, equivalent damping, and self-centering properties of the SMAs in a superelastic state. They also investigated the effect of the number of thermomechanical training cycles (compression method) on the memory effect of hollow cylindrical Fe-Mn-Si SMA casting. They analyzed the change in SME from the microstructural perspective and attributed it mainly to the preferred orientation of martensite and the formation of winding and dislocations in the alloy crystal structure during the thermomechanical training. Qian *et al*. (2011, 2013) studied the mechanical properties of superelastic NiTi SMA wires of different diameters. They analyzed the effects of cyclic loading times, strain amplitudes, loading rates, and ambient temperature on the mechanical properties and then improved its constitutive model. Suhail *et al*. (2020a) studied the strain localization phenomenon, strain-rate effect, and interaction of NiTi SMA wires. During stress-induced martensitic transformation, the expansion of the phase transition band showed a non-uniform strain distribution, and the unloading strain recovery within the transformation bands exhibited high strain-rate sensitivity. Fang *et al*. (2019) studied the effect of heat treatment on the phase transformation characteristics and mechanical properties of SMA cables, performed cyclic loading tests at room temperature, and studied further development of the mechanical behaviors of the SMA cables. Suhail *et al*. (2020b) studied the recovery stress generated by heating prestressed NiTi SMA wires and analyzed the optimal pre-strain value of the maximum recovery stress of the material.

The study of mechanical properties of SMAs lays a solid foundation for investigating their resistance sensing properties. The resistance of the SMA sensing element changes with the macroscopic strain or stress, which can be obtained by applying the voltage and current without additional measurement equipment. Therefore, SMAs may be used to integrate monitoring and sensing in the driving system with closed-loop control. SMAs can be used as feedback with resistance sensing characteristics, which have great engineering application potential. Therefore, many experimental studies have been conducted on the resistance characteristics of SMAs.

Ikuta *et al*. (1988) proposed an antagonistic type deformation control scheme using resistance feedback, which was experimentally verified, and the suggested servo actuator system was successfully applied in an active endoscope. Novak *et al*. (2008) investigated the evolution of the resistivity of NiTi SMA wires with R-phase transformation during thermal and mechanical tests using experiments and micromechanical model simulations. Sreekanth *et al*. (2018) investigated the considerable strain shown by SMAs during phase transformation with temperature. They demonstrated that the current rise time through a helical spring is directly proportional to its displacement and proposed a method to obtain the temperature of the SMA during actuation by estimating the resistance from the rise time. Zhang *et al*. (2013) explored and modeled the self-sensing properties of SMAs to imitate the integrated muscle-like functions of actuating and self-sensing based on the investigation of the electrical resistivity of SMAs. They verified the validity of the electrical resistance (ER) model by conducting a series of thermal–electrical–mechanical experiments. Mohan and Banerjee (2021) proposed a novel yield parameter, which enables accurate simulation of minor hysteresis loop using the model of Boyd and Lagoudas. Using the modified model, pseudoelastic responses are compared against those obtained from the existing models, which illustrates its efficacy. Jain *et al*. (2020) explored the principle of significant change in the ER of SMAs during their solid-phase transformation from austenite to martensite. Sensors could be employed for the detection of variable velocity flows and for obtaining the acceleration of the flow with proper tuning of input voltage and stress. Airoldi *et al*. (1996) examined the ER of NiTiCu ribbons either in the pseudoelastic range in martensite or under constant applied stress across the transformation range. The results show that the ER follows a linear relationship with the imprinted strain. Sherif and Ozbulut (2020) investigated the thermomechanical and electrical response of a NiTi SMA cable with a distinctive configuration, which was subjected to cyclic loading at various strain amplitudes ranging from 3 to 7%. The results show that the global ER change cannot predict the strain/stress state accurately because of the complex geometry of the cable. Song *et al*. (2006) fabricated a concrete beam specimen with SMA reinforcing cables and embedded PZT patches. Experiments demonstrated that the IRC possesses self-sensing and self-rehabilitation capabilities. The crack width of the specimen can be estimated by monitoring the electric resistance change of the SMA cables. Lee *et al*. (2020) also added an SMA and carbon fiber-reinforced polymer into the beam and used the resistance of the SMA as a feedback signal for estimating self-sensed deflection. The deflection was well controlled; however, its response was slightly delayed.

In summary, many studies have explored the excellent mechanical and resistance sensing characteristics of SMAs. However, the use of SMAs as sensing elements needs further investigation. In this study, the mechanical and resistance sensing characteristics of superfine wires made of SMA (which is martensite at room temperature) were investigated. This study aimed to explore the relationship between strain, stress, and resistance of superfine SMA wires during phase transformation. The results of experiments can form the basis for the application of superfine SMA wires.

2. Materials and test setup

2.1 Materials

In this experiment, NiTi SMA wires with a diameter of 25 μm (SAES Smart Materials, USA) were used. Table 1 shows the elemental composition of the SMA wires (by mass).

The phase transition temperature of the material was measured using differential scanning calorimetry (DSC; DSC204, NETZSCH, Germany). The analysis results are

Table 1 Chemical composition of the SMA

Chemical composition	Mass percentage %/wt.
Ni	55.8 ± 0.5
Ti	42.6 ± 0.5
C	≤ 0.05
H	≤ 0.005
O	≤ 0.05
Fe	≤ 0.05
others	≤ 0.01

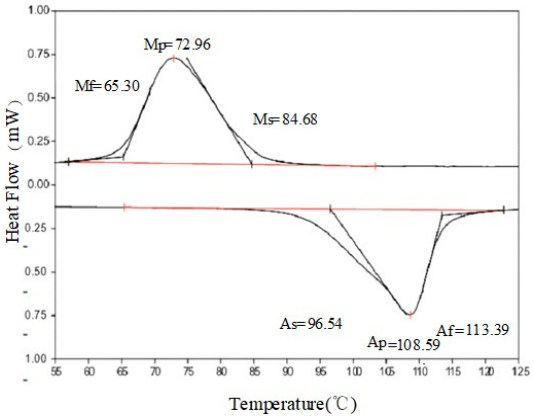

Fig. 1 DSC curves of SMA wires

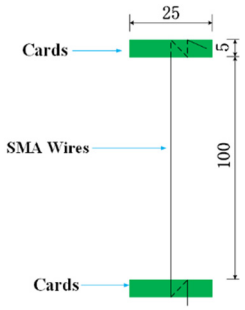

Fig. 2 Specimen

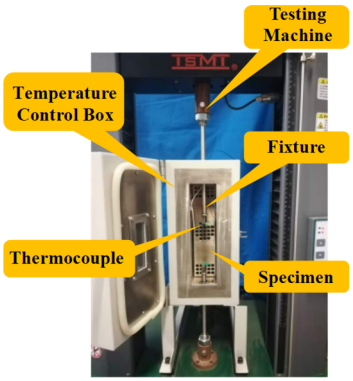

Fig. 3 Experimental setup

shown in Fig. 1. The following phase transition temperatures of the material were identified: M_f = 65.3°C, M_s = 84.6°C, A_s = 96.5°C, and A_f = 113.4°C.

As shown in Fig. 2, the length of the SMA wires used was 140 mm. To prevent relaxation and slip during the tensile process, 20 mm at both ends of the SMA wires were fixed and glued to the paper. Therefore, the gauge length of the martensite specimens was 100 mm at room temperature. In addition, the specimens were dislocation-wound to prevent the wire crossing, which would affect the measurement results; the measuring end fixed at the edge of the paper was reserved to make sure that the specimens are convenient to use in a special fixture for contact and measurement.

2.2 Experimental setup

The experimental setup and equipment used are shown in Fig. 3. The experimental apparatus was composed of measuring and data acquisition systems. The measuring system included a material tensile testing machine and measuring device. The stress–strain relationship of superfine SMA wires was measured using an electromechanical universal testing machine. The ER of superfine SMA wires was measured using a four-wire method. During measurement, the current did not pass through the voltmeter to ensure the accuracy of the measurement results. A high-precision DC tester (TM2516, Shenzhen Instrument Co., Ltd., China) with a resistance measuring range of 1 μΩ–200 kΩ and resistance measuring accuracy of 0.05% was connected to the testing machine through the expansion port, which enabled the synchronous acquisition of SMA resistance and tensile test data.

3. Experimental procedure and analysis methods

3.1 Experimental procedure

Many scholars have found that the mechanical properties of SMA wire and rod will gradually stabilize in uniaxial cyclic tensile test. We describe this phenomenon as training process. During training (cyclic loading and unloading), the number of cycles considerably affects the behavior of SMA, worsening the energy dissipation capability and increasing the cyclic strain hardening. However, these properties stabilize after a certain number of cycles. In this part of the experiment, during training, each specimen was repeatedly loaded to the set amplitude and unloaded to the initial state using the hyperelasticity of austenite. After that, the effects of cyclic training time and training strain amplitude on the following mechanical properties: stress–strain relationship, hysteretic energy dissipation capacity, secant stiffness, equivalent damping ratio, and residual strain during specimen training were mainly considered. The mechanical properties of superfine SMA wires under three sets of working conditions were studied:

(1) The initial training of the austenitic SMA. To ensure the stability of the mechanical properties of SMA wires, uniaxial cyclic tensile tests were performed. The effects of training strain amplitudes and training time on the mechanical properties of superfine SMA wires were

investigated. The training strain amplitudes were 4, 6, and 8%. The temperature at 120°C was maintained during the test, and the loading strain rate was 0.005 s^{-1}.

(2) Uniaxial tensile test of the austenitic SMA. This part was conducted to compare the mechanical properties of superfine SMA wires after the training at different amplitudes. During the test, the temperature was maintained at 120°C, the strain amplitude was 4%, and the loading strain rate was 0.005 s^{-1}.

(3) Uniaxial tensile test of the martensitic SMA. This part was conducted to analyze the effects of training strain amplitude and cyclic loading time on the mechanical properties of the martensitic SMA. During the test, the temperature was maintained at 40°C, the strain amplitude was 4%, and the loading strain rate was 0.001 s^{-1}.

3.2 Methods of mechanical property analysis

Fig. 4 shows the typical stress–strain curves and characteristic parameters of SMAs corresponding to single loading and unloading cycles, where σ_{Ms}, σ_{Mf}, σA_s, and σ_{Af} represent the beginning stress of martensitic transformation, end stress of martensitic transformation, beginning stress of austenite transformation, and end stress of austenite transformation, respectively. To analyze the mechanical properties of SMA filaments under different working conditions, the following mechanical characteristic parameters were defined:

(1) Cyclic energy dissipation capacity W_D: the area enclosed by the stress–strain curve during one loading and unloading (curve OABCDEFO), which represents the hysteretic energy dissipation capacity of an SMA.

(2) Secant stiffness k_S: the ratio of peak load to maximum displacement, as shown in Eq. (1).

$$k_s = \frac{F_{max} - F_{min}}{\delta_{max} - \delta_{min}} \tag{1}$$

(3) Equivalent damping ratio ξ_{eq}: the damping ratio of the SMA under unloading conditions after the uniaxial tensile process reflects the damping performance of the SMA, where W_E is the total strain energy of a single cycle, equal to the sum of W_D and W, as shown in Eq. (2).

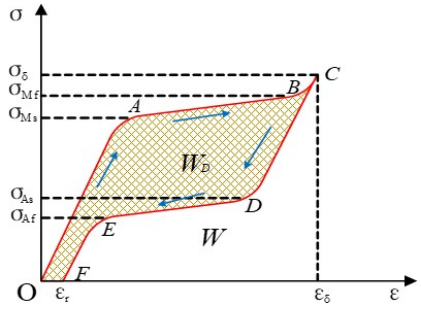

Fig. 4 Schematic stress–strain curves and mechanical parameters of austenitic SMAs

$$\xi_{eq} = \frac{W_D}{4\pi W_E} = \frac{W_D}{2\pi k_s \varepsilon_\delta^2} \tag{2}$$

(4) Residual strain ε_r: the corresponding strain value of the specimen when unloading to zero stress (to evaluate the self-centering ability of the SMA).

3.3 Methods of ER sensing analysis

Based on the mechanical test results, the ER sensing test was carried out with the trained specimen. The strain-sensing test of superfine SMA wires consisted of a tensile test and resistance measurement. To enrich the resistance test data of the material and ensure the stability of the mechanical properties of the SMA filament, a specimen with a training strain amplitude of 8% was used for the test. In this experiment, an important indicator of resistance characteristics, resistance variation in Eq. (3), was studied from the following three aspects: the strain-sensing characteristics, the effect of loading rate on resistance, and the effect of temperature on resistance.

$$\Delta R = \frac{R - R_0}{R_0} \tag{3}$$

where R_0 is the initial resistance of the SMA specimen, R is the measured resistance, and ΔR is the resistance variation.

4. Experimental results and discussion

4.1 Analysis of ER sensing characteristics

In general, the NiTi SMA has three phases: martensitic, austenitic, and R. These three phases have different resistivities. During phase transformation, the volume percentage of each phase changes. Therefore, we assumed the volume percentage content of each phase to be ξ_A, ξ_M, ξ_R, and the resistivity: ρ_A, ρ_M, ρ_R, respectively. Ikuta *et al.* (1991) reported that all phases of SMA are randomly distributed at the microscopic scale but can be regarded as parallelly distributed at the macroscopic scale, as shown in Fig. 5. Using this variable sublayer model, Dutta and Ghorbel (2005) proposed nonlinear temperature coefficients of resistivity for each phase to model SMA resistance. Therefore, the linear summation relationship shown in Eq. (4) holds for the resistivity of each phase. Moreover, Fig. 2 indicates that the superfine SMA wires did not contain the R phase, which was thus not considered in the present study.

$$\rho = \rho_A + \rho_M + \rho_R \tag{4}$$

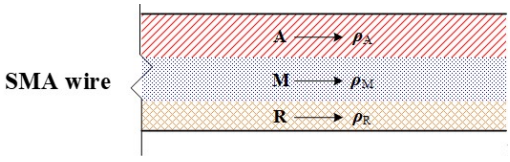

Fig. 5 Variable sublayer model of SMA

4.2 Mechanical behaviors of superfine SMA wires

4.2.1 Effect of cyclic loading on mechanical properties

The stability of mechanical properties of SMAs is the basis of their application in practical engineering. Current studies have shown that the mechanical properties of austenitic SMA would gradually stabilize under cyclic loading. To explore the effect of training on the mechanical properties of superfine martensitic SMA wires, a test was designed with the cyclic loading and unloading of a single virgin specimen. During the test, the temperature was maintained at 120°C, fixed loading strain amplitude was 4%, and loading strain rate was 0.005 s^{-1}. When the set number of training cycles was reached (1, 10, 20, 30, 40, and 50), the test was stopped, and the temperature was decreased to 40°C. After that, uniaxial tensile tests of the SMA in a complete martensitic state were conducted to analyze the variation of the stress–strain curve of the martensitic SMA corresponding to high-temperature training.

Fig. 6 shows the stress–strain curve of the austenitic SMA wire after different numbers of cycles at 120°C. With the increase in the number of cycles, the initial martensitic transformation stress of the superelastic specimen gradually decreased and then stabilized. In this process, the stress–strain curve gradually changes from the initial flag type to the fusiform type. Moreover, the hysteretic energy dissipation capacity decreased from 896.21 $MJ \cdot m^{-3}$ in the first round to 431.97 $MJ \cdot m^{-3}$ in the 50th round, and the overall decrease was approximately 48.2%. At the same time, the loading and unloading stages tended to stabilize after 40 cycles. As shown in Fig. 6, the specimen did not slip during the test, which proved the reliability of the clamping scheme.

Fig. 7 shows the stress–strain curve of the martensitic SMA under different numbers of training cycles at 40°C. The figure shows that the peak stress of the stress–strain curve increases with the number of training cycles, implying that the strain energy of the wire also increases. The specimen, in complete martensitic state at 40°C is mainly composed of twinned martensite and detwinned martensite. Detwinned martensite crystals have a higher elastic modulus than twinned martensite crystals. During loading, stress induced the transformation of twinned martensite into detwinned martensite with a more favorable direction, that is, twinning occurred. With the increasing number of training cycles, the volume fraction of detwinned martensite increases, resulting in the continuous shortening of the twinning stage. In Figs. 6 and 7, the test curves of the 40th and 50th turns are almost the same, indicating that the mechanical properties of austenitic and martensitic SMA filaments can stabilize at the same time under high-temperature cyclic training.

Mechanical properties of the martensitic SMA under different numbers of training cycles are shown in Table 2. With an increasing training period, during the gradual stabilization of the specimen, the hysteretic energy increases by approximately 11%. The peak stress and equivalent secant stiffness significantly increased, and the secant stiffness increased by approximately 150%. Residual strain and damping ratio gradually decreased by 17 and 56%, respectively.

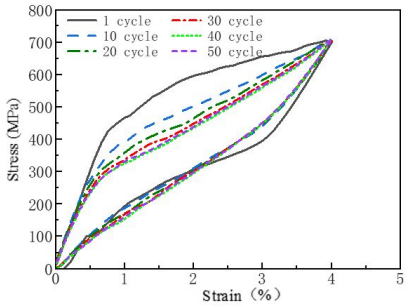

Fig. 6 Stress–strain curves of the SMA wire under increasing cyclic load

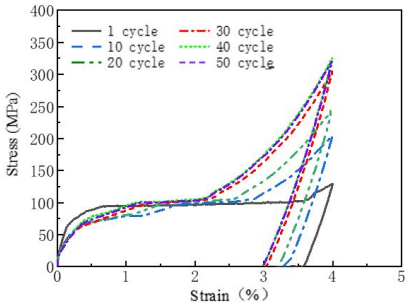

Fig. 7 Stress–strain curves of the martensitic SMA with corresponding cycles

Table 2 Characteristic parameters of the martensitic SMA at different numbers of cycles

Training cycles	Hysteretic energy ($MJ \cdot m^{-3}$)	Residual strain (%)	Peak stress (MPa)	Equivalent secant stiffness (GPa)	Damping ratio (%)
1	3.56	3.57	128.8	3.2	11.1
5	3.79	3.51	154.6	3.8	9.7
10	3.46	3.33	203.1	5.1	6.8
20	3.62	3.21	245.0	6.1	5.9
30	3.83	3.03	305.7	7.6	5.0
40	3.97	2.97	323.6	8.1	4.9
50	3.91	2.97	323.5	8.1	4.8

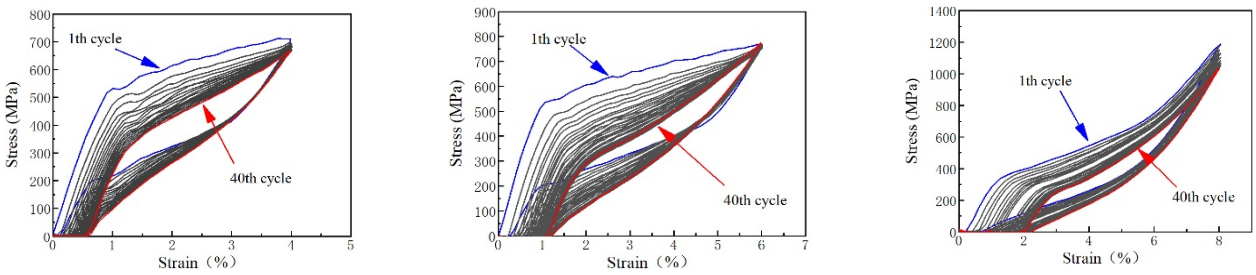

(a) 4% (b) 6% (c) 8%

Fig. 8 Training of the austenitic NiTi SMA at different strain amplitudes

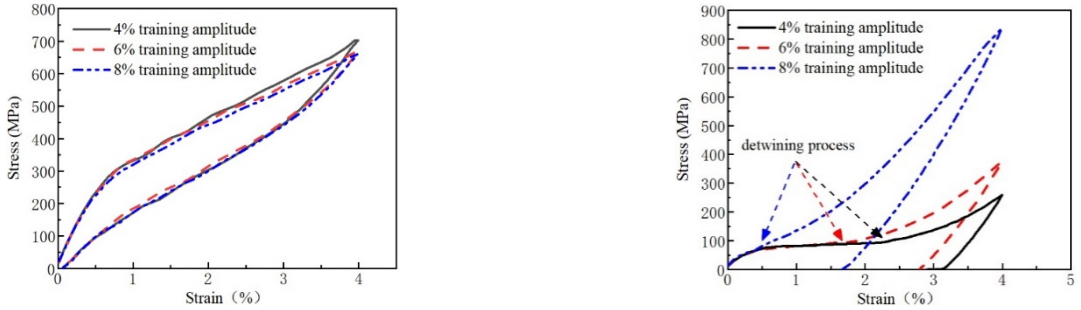

(a) Austenite (b) Martensite

Fig. 9 Stress–strain curves of specimens after training

4.2.2 Effect of training amplitude on mechanical properties

The specimens were trained with strain amplitudes of 4, 6, and 8% at the temperature of 120°C and a loading rate of 0.005 s^{-1}, and the results are illustrated in Fig. 8. With increasing training strain amplitude, the residual strain gradually increased because of the accumulation of dislocations in the crystal structure during training. After 40 cycles, the mechanical properties of superelastic specimens stabilized.

Fig. 9 shows the stress–strain curves of austenitic and martensitic SMA specimens after training. Upon completion of the training, the uniaxial tensile tests of the austenitic SMA specimens were conducted at the temperature of 120°C, amplitude of 4%, and loading strain rate of 0.005 s^{-1}, and then the stress–strain curve was obtained (Fig. 9(a)). The specimens with different training strain amplitudes exhibited almost the same stress–strain curves. Thus, it can be concluded that the training strain amplitude has a weaker effect on the superelastic behavior of the material.

The next section describes the analysis of the properties of the martensitic SMA. After the training of each specimen, the martensitic SMA uniaxial tensile tests were conducted at the temperature of 40°C, amplitude of 4%, and loading strain rate of 0.001 s^{-1}. The stress–strain curves are shown in Fig. 9(b). With increasing training strain amplitude, the hysteretic energy and equivalent secant stiffness of the specimens increased during training. Fig. 10 shows the elastic modulus of each specimen in Fig. 8 during loading. With increasing training amplitude, the turning point of elastic modulus (2, 1.6, and 0.4% for amplitudes of 4, 6, and 8% respectively) gradually decreased. This indicates that the volume fraction of the detwinned

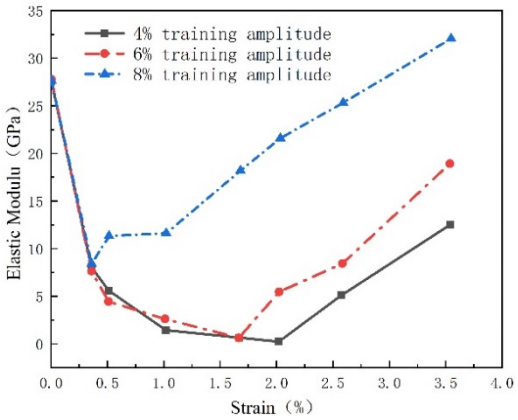

Fig. 10 Variation in elastic modulus of each martensitic specimen during loading

martensite at the temperature below M_f increased with the strain amplitude, which resulted in the shortening of the detwinning stage, and earlier completion of the stress-induced martensitic transformation. Thus, the elastic modulus of the material increased sharply, and the mechanical properties of the martensitic SMA changed.

Table 3 shows the mechanical properties of the martensitic specimens after training. With the increase in the training strain amplitude from 4 to 8%, the hysteretic energy increased by approximately 63%. The peak stress and equivalent secant stiffness also increased significantly. As shown below, the equivalent secant stiffness increased by approximately 325%. However, the residual strain decreased from 3.15 to 1.68%, while the damping ratio decreased by approximately 50%.

Table 3 Characteristic parameters of specimens at 40°C after training

Training amplitude	Training cycles	Peak stress (MPa)	Equivalent secant stiffness (GPa)	Damping ratio (%)	Residual strain (%)	Hysteretic energy ($MJ·m^{-3}$)
4%	50	258.5	6.5	5.1	3.15	3.3285
6%	50	380.5	9.5	3.7	2.78	3.5348
8%	50	841.7	21.1	2.6	1.68	5.4211

Table 4 Schemes of ER sensing experiments

Test schemes	Pre-trained amplitude (%)	Tensilestrain amplitude (%)	Loading rate (s^{-1})	Test temperature (°C)
1	8	5	0.003	40–120
2	8	5	0.001, 0.003, 0.005	-30–120

4.3 ER sensing of superfine SMA wires

The stability of mechanical properties needs to be determined to thoroughly utilize the resistance sensing ability of superfine SMA wires. To make sure the accuracy of the test results of super-fine SMA wires, we conducted a large number of pre-experiments. As determined by several tests, the accuracy of the SMA specimen resistance test results can be guaranteed within the 5% strain amplitude. Therefore, a specimen trained at 8% strain amplitude was used for the resistance characteristics tests in this study. By considering the influence of loading rates and temperatures on ER sensing characteristics, the test schemes are shown in Table 4. As a result of using pre-trained specimens and eliminating recoverable residual strain by heating up to A_f after each test.

4.3.1 ER sensing at different temperatures

First, the strain-sensing properties of SMA filaments, which are martensitic at lower temperatures, needed to be

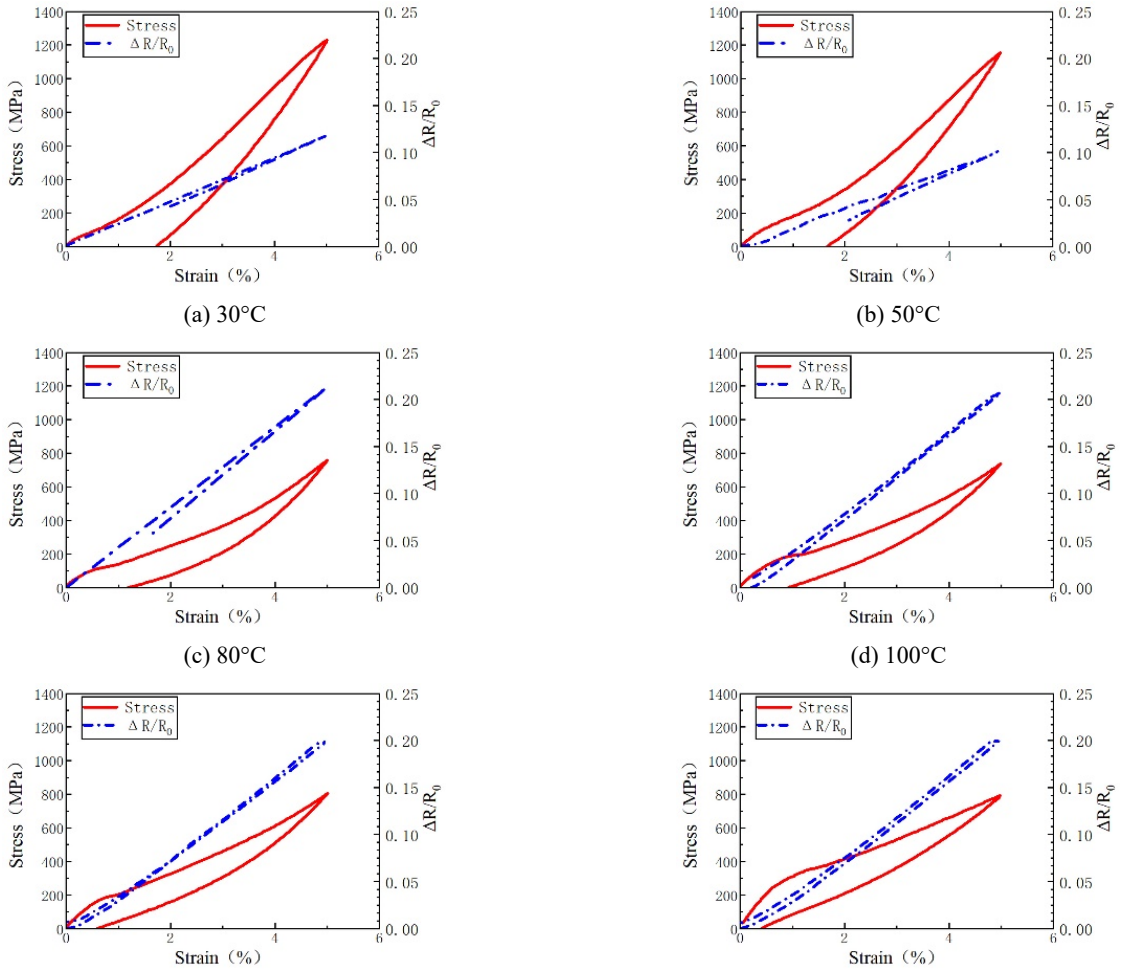

(a) 30°C (b) 50°C

(c) 80°C (d) 100°C

(e) 110°C (f) 120°C

Fig. 11 Stress–strain curves and relative resistance–strain curves of superfine SMA wires at different temperatures

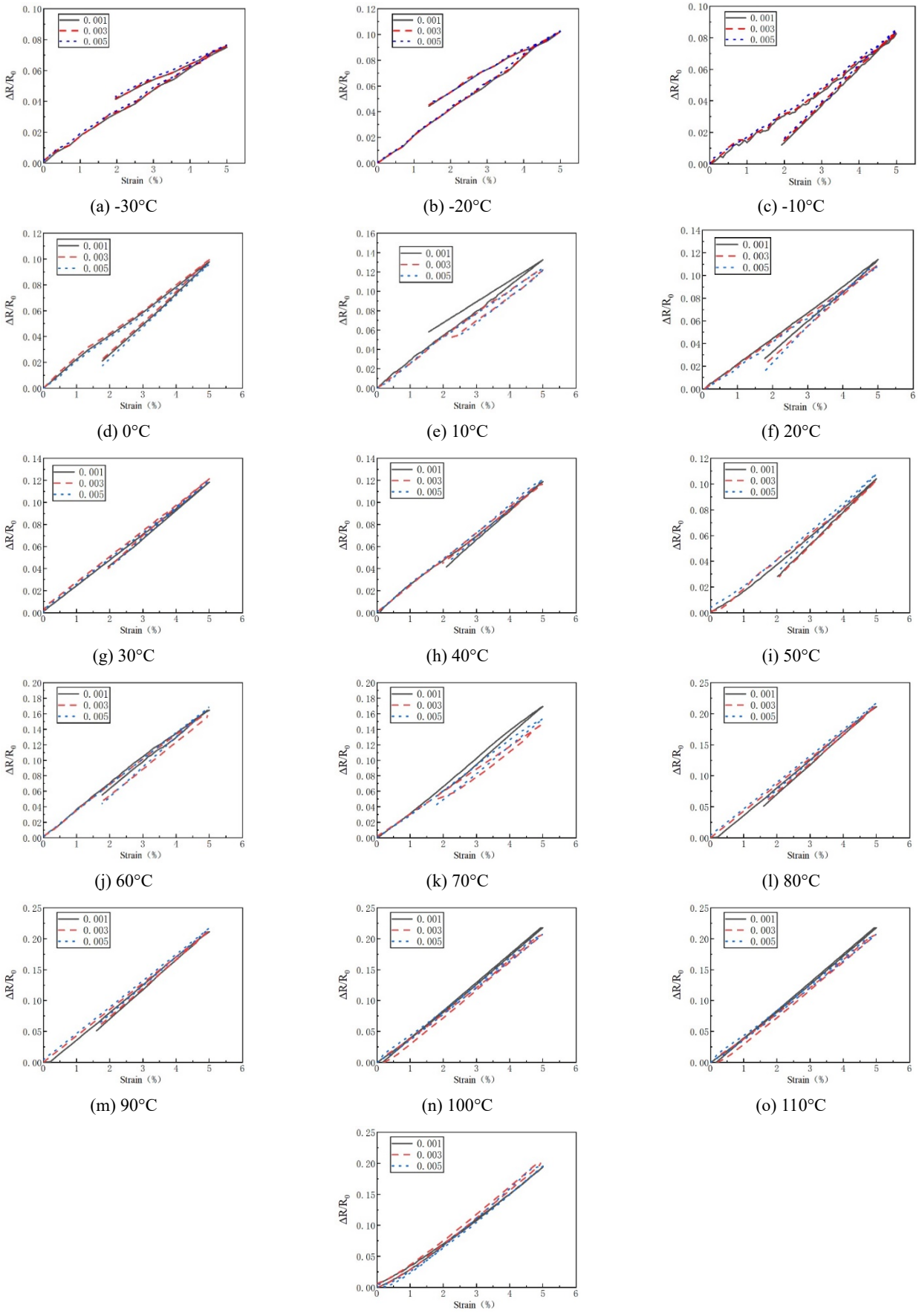

(a) -30°C (b) -20°C (c) -10°C

(d) 0°C (e) 10°C (f) 20°C

(g) 30°C (h) 40°C (i) 50°C

(j) 60°C (k) 70°C (l) 80°C

(m) 90°C (n) 100°C (o) 110°C

(p) 120°C

Fig. 12 Effect of loading rate on the resistance variation of superfine SMA wires

confirmed, so the resistance of the specimen was tested at different temperatures from 40 to 120°C.

Fig. 11 shows the relationship between the stress–strain and ER resistance–strain curves for the SMA specimens (trained at 8% strain amplitude) at different temperatures. As shown in Fig. 11, when the temperature exceeds 70°C, SMA filaments begin to transform from the initial martensitic phase to the austenitic phase, yield platform of the stress–strain relationship curve gradually rises, and residual deformation decreases after unloading. At 120°C, the SMA is completely in the austenite phase, and the residual deformation is about 0.4% (see the stress scale on the left).

In general, the resistance of the SMA filament in the martensitic phase and the phase transformation is linearly related to the strain. However, the resistance variation of the austenitic SMA filament in the elastic stage was relatively low (see the resistance variation scale on the right). After that, with increasing tensile stress, the material underwent stress-induced martensitic transformation and the resistance variation slightly increased, which resulted in a piece-wise linear relationship.

4.3.2 ER sensing under different loading rates

The application of SMA superfine wires in practical engineering requires sufficient test data; therefore, comprehensive consideration should be given to the test conditions. In this experiment, we investigated the effect of loading rate on the resistance of superfine SMA wires, and considering the actual working environment, the test temperature range was expanded to -30–120°C. The low-temperature environment was realized using liquid nitrogen.

The effect of loading rate on the resistance of superfine SMA wires is shown in Fig. 12. Owing to the generation of residual strain in the tensile process, the resistance characteristics of the loading and unloading sections were different. Considering the experimental error, the resistance of superfine SMA wires may be considered to exhibit an excellent linear correlation with strain. At the same time, the loading rate had little effect on the resistance variation of the specimen at the same temperature, still maintaining a good linear relationship. This phenomenon greatly simplifies the establishment of the resistance characteristic model of SMA filaments in actual engineering.

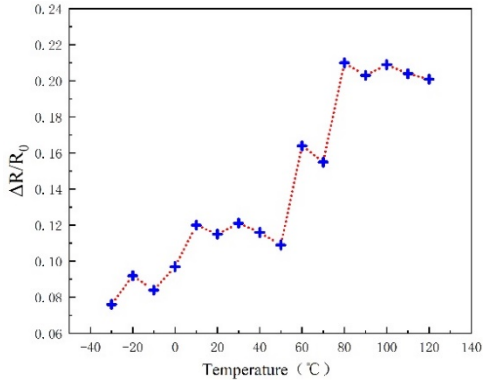

Fig. 13 Effect of Temperature on ER Characteristics of Superfine SMA Wires

Fig. 13 shows the changes in the maximum resistance variation of SMA filaments with increasing temperature. With the gradual increase in temperature, the maximum resistance variation of SMA filaments overall increases. In the temperature ranges of 10–50°C and 90–120°C, the SMA filament is in the state of complete martensite and austenite, respectively. The resistance variation of the material fluctuates forming two platforms. During the phase transition between the two platforms, the resistance variation increases significantly, so it can be judged that the resistance variation of austenitic SMA is higher than that of martensitic SMA by approximately 1.8 times.

5. Conclusions

Thermomechanical and electrical sensing characteristics of superfine SMA wires were investigated in this study. To obtain stable mechanical properties of SMA wires, specimens were trained in the austenite state at 120°C using uniaxial cyclic loading and unloading. The loading and unloading strain amplitude in the training process was determined according to the purpose of the test scheme. The experimental results show that superfine SMA wires can be used as stable sensing elements with the linear relationship between resistance and strain. Therefore, this material has great engineering application potential. The major conclusions are summarized below.

- The mechanical properties of austenite and martensite can be stabilized simultaneously through cyclic loading training in the austenitic state at high temperatures.
- With the increase of the training strain amplitude, the increases in the volume fraction of detwinned martensite in the SMA at low temperatures results in shortening of the twinning process, which significant increases in the hysteretic energy dissipation capacity and tangent stiffness and reduces in the damping ratio and residual deformation.
- The results of ER sensing experiment show that the strain-sensing characteristics of austenitic superfine SMA wires are piece-wise linear and that the strain–resistance curves of martensitic superfine SMA wires exhibit excellent linear correlation. Therefore, this material may be used for the manufacturing of sensitive displacement sensors and applied in structural health monitoring.
- The experimental results show that the effect of loading rate on the mechanical properties and resistance sensing characteristics of superfine SMA wires can be ignored. This finding indicates that superfine SMA wires have a large specific surface area, through which latent heat is rapidly dissipated into the environment, thus ensuring the stability of the internal temperature of the material during the tensile process.

Acknowledgments

This work was supported by the National Natural Science Foundation of China (Project codes: 51978631). The authors also appreciate Henan Haoze Electronics Co. Ltd for providing the superfine SMA wires, and the help from Mrs. Liping KANG and Mr. Yifei SHI during the experiments.

References

Airoldi, G., Pozzi, M. and Riva, G. (1996), "The electrical resistance properties of shape memory alloys", *MRS Online Proceedings Library*. https://doi.org/10.1557/PROC-459-459

Casciati, S. and Marzi, A. (2010), "Experimental studies on the fatigue life of shape memory alloy bars", *Smart Struct. Syst., Int. J.*, **6**(1), 73-85. https://doi.org/10.12989/sss.2010.6.1.073

Churchill, C.B., Shaw, J.A. and Iadicola, M.A. (2010), Tips and tricks for characterizing shape memory alloy wire: Part 4–thermo-mechanical coupling.

Cui, D., Song, G. and Li, H. (2010), "Modeling of the electrical resistance of shape memory alloy wires", *Smart Mater. Struct.*, 55019. https://doi.org/10.1088/0964-1726/19/5/055019

DesRoches, R., McCormick, J. and Delemont, M. (2004), "Cyclic properties of superelastic shape memory alloy wires and bars", *J. Struct. Eng.*, **130**(1), 38-46.

Dhanalakshmi, K., Umapathy, M., Ezhilarasi, D. and Bandyopadhyay, B. (2011), "Design and implementation of fast output sampling feedback control for shape memory alloy actuated structures", *Smart Struct. Syst., Int. J.*, **8**(4), 367-384. https://doi.org/10.12989/sss.2011.8.4.367

Dolce, M. and Cardone, D. (2001a), "Mechanical behaviour of shape memory alloys for seismic applications 1. Martensite and austenite NiTi bars subjected to torsion", *Int. J. Mech. Sci.*, **43**(11), 2631-2656. https://doi.org/10.1016/S0020-7403(01)00049-2

Dolce, M. and Cardone, D. (2001b), "Mechanical behaviour of shape memory alloys for seismic applications 2. Austenite NiTi wires subjected to tension", *Int. J. Mech. Sci.*, **43**(11), 2657-2677. https://doi.org/10.1016/S0020-7403(01)00050-9

Dutta, S.M. and Ghorbel, F.H. (2005), "Differential hysteresis modeling of a shape memory alloy wire actuator", *IEEE/ASME Transact. Mechatron.*, **10**(2), 189-197. https://doi.org/10.1109/TMECH.2005.844709

Fang, C., Zheng, Y., Chen, J., Yam, M.C. and Wang, W. (2019), "Superelastic NiTi SMA cables: Thermal-mechanical behavior, hysteretic modelling and seismic application", *Eng. Struct.*, **183**, 533-549. https://doi.org/10.1016/j.engstruct.2019.01.049

Ikuta, K., Tsukamoto, M. and Hirose, S. (1988), "Shape memory alloy servo actuator system with electric resistance feedback and application for active endoscope", *Proceedings of 1988 IEEE International Conference on Robotics and Automation*, Philadelphia, PA, USA, April, pp. 427-430.

Ikuta, K., Tsukamoto, M. and Hirose, S. (1991), "Mathematical model and experimental verification of shape memory alloy for designing micro actuator", *IEEE Micro Electro Mech. Syst.*, 103-108. https://doi.org/10.1109/MEMSYS.1991.114778

Jain, A.K., Sharma, A.K., Khandekar, S. and Bhattacharya, B. (2020), "Shape Memory Alloy-Based Sensor for Two-Phase Flow Detection", *IEEE Sens. J.*, **20**(23), 14209-14217. https://doi.org/10.1109/JSEN.2020.3008191

Janke, L., Czaderski, C., Motavalli, M. and Ruth, J. (2005), "Applications of shape memory alloys in civil engineering structures - Overview, limits and new ideas", *Mater. Struct.*, **38**(5), 578-592. https://doi.org/10.1617/14323

Lee, S.H. and Kim, S.W. (2020), "Self-sensing-based deflection control of carbon fibre-reinforced polymer (CFRP)-based shape memory alloy hybrid composite beams", *Compos. Struct.*, **251**, 112544. https://doi.org/10.1016/j.compstruct.2020.112544

Lee, H.T., Kim, M.S., Lee, G.Y., Kim, C.S. and Ahn, S.H. (2018), "Shape memory alloy (sma)-based microscale actuators with 60% deformation rate and 1.6 kHz actuation speed", *Small*, **14**(23), 1801023. https://doi.org/10.1002/smll.201801023

Lee, H.T., Seichepine, F. and Yang, G.Z. (2020), "Microtentacle actuators based on shape memory alloy smart soft composite", *Adv. Funct. Mater.*, **30**(34), 2002510. https://doi.org/10.1002/adfm.202002510

Lester, B.T., Baxevanis, T., Chemisky, Y. and Lagoudas, D.C. (2015), "Review and perspectives: shape memory alloy composite systems", *Acta Mech.*, **226**, 3907-3960. https://doi.org/10.1007/s00707-015-1433-0

Mohan, S. and Banerjee, A. (2021), "Modelling of minor hysteresis loop of shape memory alloy wire actuator and its application in self-sensing", *Smart Mater. Struct.*, **30**(5), 055011. https://doi.org/10.1088/1361-665X/abeefa

Nahm, S.H., Kim, Y.J., Kim, J.M. and Yoon, D.J. (2005), "A study on the application of Ni-Ti shape memory alloy as a sensor", In: *Materials Science Forum*, Vol. 475, pp. 21043-2046. https://doi.org/10.4028/www.scientific.net/MSF.475-479.2043

Nakshatharan, S. and Dhanalakshmi, K. (2014), "Differential resistance feedback control of a self-sensing shape memory alloy actuated system", *ISA Trans.*, **53**(2), 289-297. https://doi.org/10.1016/j.isatra.2013.11.002

Novák, V., Šittner, P., Dayananda, G.N., Braz-Fernandes, F.M. and Mahesh, K.K. (2008), "Electric resistance variation of NiTi shape memory alloy wires in thermomechanical tests: Experiments and simulation", *Mater. Sci. Eng.: A*, **481**, 127-133. https://doi.org/10.1016/j.msea.2007.02.162

Qian, H., Li, H.N., Song, G.B. and Chen, H. (2011), "Dynamical behavior and constitutive model of superelasticity niti shape memory alloy wire: experiment and theory", *J. Solid Mech.*, **32**(04), 353-359. [In Chinese]

Qian, H., Li, J.B., Li, H.N. and Chen, H. (2013), "Mechanical behavior tests of NiTi wires with different diameters for structural vibration control", *J. Vib. Shock*, **32**(24), 89-95. [In Chinese]

Sherif, M.M. and Ozbulut, O.E. (2020), "Thermomechanical and electrical response of a superelastic NiTi shape memory alloy cable", *J. Intell. Mater. Syst. Struct.*, **31**(19), 2229-2242. https://doi.org/10.1177/1045389X20943952

Shi, Z., Wang, T. and Da, L. (2014), "Performance analyses of antagonistic shape memory alloy actuators based on recovered strain", *Smart Struct. Syst., Int. J.*, **14**(5), 765-784. https://doi.org/10.12989/sss.2014.14.5.765

Song, G., Mo, Y.L., Otero, K. and Gu, H. (2006), "Health monitoring and rehabilitation of a concrete structure using intelligent materials", *Smart Mater. Struct.*, **15**(2), 309-314. https://doi.org/10.1088/0964-1726/15/2/010

Song, G., Ma, N. and Lee, H.J. (2007), "Position estimation and control of SMA actuators based on electrical resistance measurement", *Smart Struct. Syst., Int. J.*, **3**(2), 189-200. https://doi.org/10.12989/sss.2007.3.2.189

Sreekanth, M., Mathew, A.T. and Vijayakumar, R. (2018), "A novel model-based approach for resistance estimation using rise time and sensorless position control of sub-millimetre shape memory alloy helical spring actuator", *J. Intell. Mater. Syst. Struct.*, **29**(6), 1050-1064. https://doi.org/10.1177/1045389X17730911

Suhail, R., Chen, J.F., Amato, G. and McCrum, D. (2020a), "Mechanical behaviour of NiTiNb shape memory alloy wires–strain localisation and effect of strain rate", *Mech. Mater.*, **144**,

103346. https://doi.org/10.1016/j.mechmat.2020.103346
Suhail, R., Amato, G. and McCrum, D. (2020b), "Heat-activated prestressing of NiTiNb shape memory alloy wires", *Eng. Struct.*, **206**, 110128. https://doi.org/10.1016/j.engstruct.2019.110128
Suhail, R., Amato, G. and McCrum, D. (2021), "Thermo-mechanical characterisation of NiTi-based shape memory alloy wires for civil engineering applications", *J. Intell. Mater. Syst. Struct.*, **32**(20), 2420-2436.
Zadafiya, K., Kumari, S., Chatterjee, S. and Abhishek, K. (2021), "Recent trends in non-traditional machining of shape memory alloys (SMAs): A review", *CIRP J. Manuf. Sci. Technol.*, **32**, 217-227. https://doi.org/10.1016/j.cirpj.2021.01.003
Zhang, J.J., Yin, Y.H. and Zhu, J.Y. (2013), "Electrical resistivity-based study of self-sensing properties for shape memory alloy-actuated artificial muscle", *Sensors*, **13**(10), 12958-12974. https://doi.org/10.3390/s131012958

HJ